This is the accepted manuscript made available via CHORUS. The article has been published as:

Nanosecond Freezing of Water at High Pressures: Nucleation and Growth near the Metastability Limit

Philip C. Myint, Alexander A. Chernov, Babak Sadigh, Lorin X. Benedict, Burl M. Hall, Sebastien Hamel, and Jonathan L. Belof

Phys. Rev. Lett. **121**, 155701 — Published 10 October 2018

DOI: 10.1103/PhysRevLett.121.155701

Nanosecond freezing of water at high pressures: nucleation and growth near the metastability limit

Philip C. Myint, Alexander A. Chernov, Babak Sadigh, Lorin X. Benedict, Burl M. Hall, Sebastien Hamel and Jonathan L. Belof*
Lawrence Livermore National Laboratory, Livermore, CA 94550, USA
(Dated: September 13, 2018)

The fundamental study of phase transition kinetics has motivated experimental methods toward achieving the largest degree of undercooling possible, more recently culminating in the technique of rapid, quasi-isentropic compression. This approach has been demonstrated to freeze water into the high-pressure ice VII phase on nanosecond time scales, with some experiments undergoing heterogeneous nucleation while others, in apparent contradiction, suggesting a homogeneous nucleation mode. In this study, we show through a combination of theory, simulation, and analysis of experiments that these seemingly contradictory results are in agreement when viewed from the perspective of classical nucleation theory. We find that, perhaps surprisingly, classical nucleation theory is capable of accurately predicting the solidification kinetics of ice VII formation under an extremely high driving force ($|\Delta\mu/k_{\mathrm{B}}T| \approx 1$), but only if amended by two important considerations: 1) transient nucleation and 2) separate liquid and solid temperatures. This is the first demonstration of a model that is able to reproduce the experimentally observed rapid freezing kinetics.

First-order phase transitions and their kinetics remain a fascinating topic with applications to virtually every major industry and to frontier fields like astronomy and inertial confinement fusion [1]. Despite its significance, many aspects of this topic are still largely unexplored, even for a fundamentally important substance like water at ambient pressure [2–4]. At this low pressure, it is difficult to deeply undercool liquid water [5, 6], and so the driving force for freezing is rather limited in magnitude. In contrast, water becomes deeply undercooled (by up to 150 degrees; see Figure 1) and remains as a metastable liquid for less than a microsecond in dynamic compression experiments performed over the past two decades where it is rapidly compressed along a quasi-isentrope to pressures above 1 GPa [7–14]. Some of these experiments have achieved peak pressures of above 6 GPa [10, 11, 13], and their conclusion is that water freezes almost instantaneously — within a few tens of nanoseconds — if it gets overdriven to this point along the quasi-isentrope. For this reason, the 6–7 GPa range is said to represent a metastability limit for the liquid.

The dynamic compression experiments have employed one of two techniques (see our review paper [18]): multiple-shock or ramp compression. In both techniques, a thin water sample sandwiched between two thicker solid windows is compressed from ambient conditions along the quasi-isentrope into the ice VII region of the phase diagram (Figure 1). Ice VII is a cubic high-pressure solid phase discovered over 80 years ago [19] that may be present in oceanic super-Earths [16, 17] and even in the Earth's mantle [20]. No theoretical model developed to date has been able to reproduce the rapid (sub-microsecond) liquid/ice VII transition kinetics observed in any of the experiments [18].

In this study, we show how a computational framework that couples classical nucleation theory (CNT) [21–26] and growth with hydrodynamic simulations can reproduce the transition kinetics observed in experiments where water freezes to completion rapidly at the metastability limit. We first apply CNT to explain past experimental observations which indicate that freezing at this limit occurs primarily through homogeneous nucleation. We then show that in order for simulations to reproduce experimental data, one must account for the fact that water under extreme conditions freezes into ice VII via transient nucleation and with essentially no thermal boundary layer at the solid/liquid interface.

The dynamic compression experiments can be divided into two categories, depending on the peak pressure achieved in the setup and the window material. It has been reported that if the peak pressure is around 5 GPa or less, freezing occurs over hundreds of nanoseconds, but only if the windows are made of silica and not sapphire [7–9, 12, 13]. Freezing does not occur at all on sub-microsecond time scales with sapphire windows. This material-dependent behavior suggests that at pressures of less than around 5 GPa, freezing occurs primarily

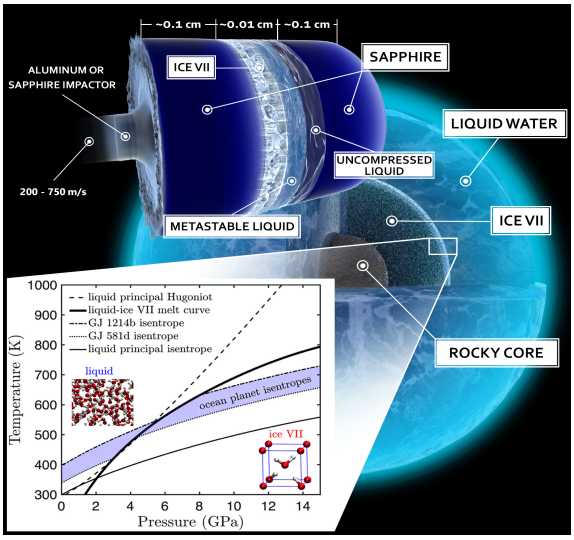

FIG. 1. Representative experimental setup for multiple-shock compression and the phase diagram for water superimposed on an illustration of a hypothetical oceanic exoplanet. The quasi-isentropic loading path before the onset of freezing to ice VII may be approximated by the liquid principal isentrope. Ice VII has a body-centered cubic (BCC) lattice of oxygen. All the curves in the phase diagram are produced from our equation of state (EOS) for the two water phases [15]. Unlike single-shock compression (where the relevant curve is the Hugoniot), quasi-isentropic compression can probe deeply undercooled states since the temperature rise along its loading path is far more attenuated. The two-phase isentropes for the oceanic super-Earths Gliese 581d (GJ 581d) and Gliese 1214b (GJ 1214b) are initiated at surface temperatures of 340 K and 400 K, respectively, which are rough estimates taken from [16] and [17].

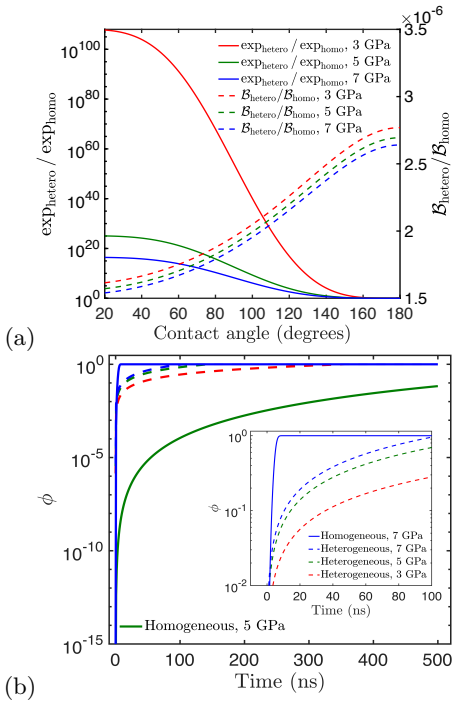

FIG. 2. (a) Ratio of exponential and pre-exponential factors for heterogeneous vs. homogeneous nucleation as a function of contact angle θ for three different pressures along the isentrope in Figure 1; (b) Comparison of the time evolution of the ice VII phase fraction ϕ for these pressures, with inset showing the behavior at early times. Freezing occurs primarily via homogeneous (heterogeneous) nucleation at higher (lower) pressures.

through heterogeneous nucleation of ice VII along the window surfaces. On the other hand, if the peak pressure goes beyond the metastability limit of 6–7 GPa, freezing achieves completion within just a few tens of nanoseconds, and it does so regardless of the window material (i.e., even with sapphire windows) [10, 11, 13]. This material-independent behavior suggests that freezing at these deeply undercooled conditions is dominated by homogeneous nucleation within the bulk of the water.

These results can be understood from the perspective of CNT. According to CNT [21–26], the steady-state homogeneous nucleation rate $J^{st}_{\rm homo}$ is given by

$$J^{st}_{\rm homo} = \mathcal{B}_{\rm homo} \exp\left(\frac{-\Delta G^*_{\rm homo}}{k_{\rm B}T}\right), \qquad (1)$$

where $\mathcal{B}_{\rm homo}$ is a pre-exponential factor that reflects the number of available nucleation sites, $\Delta G^*_{\rm homo}$ is the nucleation energy barrier, $k_{\rm B}$ is the Boltzmann constant, and T is the temperature [18]. Details regarding quantities like $\mathcal{B}_{\rm homo}$ and $\Delta G^*_{\rm homo}$ are summarized in the Supplemental Material (SM). The heterogeneous nucleation rate $J^{st}_{\rm hetero}$ may be analogously defined as $J^{st}_{\rm hetero} = \mathcal{B}_{\rm hetero} \exp\left(-\Delta G^*_{\rm hetero}/k_{\rm B}T\right)$, in which $\Delta G^*_{\rm hetero}$ is related to $\Delta G^*_{\rm homo}$ through the effective contact angle θ that ice clusters form on the water/window surface. While the detailed molecular basis for heterogeneous nucleation in this system is currently unknown, the concept of a contact angle provides an effective barrier reduction mechanism that enables analysis of the experimental results without the need to postulate specific atomistic processes.

Figure 2(a) shows that the exponential term overwhelmingly favors $J^{st}_{\rm hetero}$, especially at smaller values of θ which are indicative of better "wetting" of the window surfaces by ice than by water, but this

bias towards J^{st}_{hetero} decreases significantly at higher pressures. In contrast, the ratio $\mathcal{B}_{\text{hetero}}/\mathcal{B}_{\text{homo}}$ is relatively insensitive to the pressure and greatly favors J^{st}_{homo} since there are far more nucleation sites (i.e., water molecules) in the three-dimensional bulk of the water than along the two-dimensional window surfaces. Thus, at some sufficiently high pressure, perhaps near the metastability limit, there is a crossover where J^{st}_{homo} becomes larger than J^{st}_{hetero}. These arguments can be further understood by examining the time evolution of the ice VII phase fraction ϕ [Figure 2(b)]. The time derivative $\partial\phi/\partial t$ due to homogeneous nucleation is given by the Kolmogorov-Johnson-Mehl-Avrami (KJMA) equation [27–31] presented in Equation (6) below. At 7 GPa, the homogeneous nucleation rate is so overwhelming that the distance between the neighboring crystals is small and complete solidification is achieved after roughly 10 ns. In contrast, the solidification front in heterogeneous nucleation has to, regardless of the pressure, travel the thickness of the entire water sample, which is a much longer distance. Thus, even if we assume instantaneous saturation of the two water/window surfaces of the setup, the upper-bound limit on ϕ_{hetero} is $\phi_{\text{hetero}} = 2\gamma t/\ell$, where γ is the cluster growth rate (see Equation (2) below) and $\ell = 0.01$ cm is a representative thickness.

The CNT-based analysis underlying the results in Figure 2 seems promising in that it explains the major experimental finding that homogeneous (heterogeneous) nucleation is dominant at higher (lower) pressures. But in order to pursue a quantitative comparison with data from the experiments, a computational framework that includes coupling between CNT and hydrodynamics is required. In what follows, we describe how such a framework yields quantitative agreement with observed pressure wave profiles from all experiments conducted to date where the peak pressure exceeds the 6–7 GPa metastability limit so that homogeneous nucleation dominates. Two self-consistent features must be included to account for the deeply undercooled states present in the experiments: 1) a dual-temperature model for the liquid and ice VII phases and 2) relaxing the assumption of steady-state nucleation.

To clarify why the liquid and solid phases exist at two distinct temperatures, we note that at 7 GPa the undercooling of the liquid $\Delta T_U \approx 150$ K (Figure 1) and the latent heating by solidification is $\Delta T_Q = \Delta H/C_p \approx 100$ K [see Figure 3(b)], where ΔH is the enthalpy of fusion and C_p is the liquid isobaric heat capacity. Since $\Delta T_U > \Delta T_Q$, we have the unique scenario that the vast majority of heat released by the solidification process is absorbed by the growing crystal. As a result, the liquid must remain at a lower temperature than the newly formed ice, close to what it would be if there were no transition, thus enhancing the nucleation rate by maintaining the initial level of undercooling. We refer to this tracking of separate liquid and ice temperatures as the dual-temperature model. Furthermore, the growth rate γ of the clusters may be approximated as [32, 33]

$$\gamma = \left(\frac{k_{\text{B}}T}{m}\right)^{1/2} \frac{\Delta\mu}{k_{\text{B}}T}, \tag{2}$$

where m is the molecular mass and $\Delta\mu = \mu_{\text{solid}} - \mu_{\text{liquid}}$ is the bulk chemical potential difference. Analysis of the transport properties near the interface reveals that the growth mode is dominated by attachment kinetics (see the SM) and supports (2) as a physical description of the interface velocity.

Even at ambient pressure where metastable phases may last for a relatively long time with rapid cooling, there may not be sufficient time for steady-state nucleation to be established [34]. As a result, a transient nucleation factor [35] must be included so that the total homogeneous nucleation rate J is

$$J(t) = (1-\phi)I(t)J^{st}_{\text{homo}}. \tag{3}$$

The time-dependence of $I(t)$ suppresses nucleation at early times ($I \ll 1$), a phenomena commonly known as transient nucleation [21–26]. It is therefore not surprising that in rapid freezing under dynamic compression — where the effective cooling rate along the isentrope can exceed an extremely high value of 10^9 K/s — one must account for $I(t)$ as well. Following Kashchiev [36], we take

$$I(t) = 1 + 2\sum_{k=1}^{\infty}(-1)^k \exp\left(\frac{-k^2 t}{\tau}\right), \tag{4}$$

where the induction time τ describes the mean first passage time for crossing the region of critical cluster size within $k_B T$ of the nucleation energy barrier:

$$\tau = \zeta\frac{8k_{\text{B}}T}{\pi^2\lambda D^*}. \tag{5}$$

Here, ζ is an adjustable parameter, λ is the curvature at the top of the nucleation barrier, and D^* is an attachment rate (see the SM). If we set ζ, which

is the only free parameter in our model, equal to unity, Equation (5) reduces to the classical expression obtained by Kashchiev. Simulations with our model, applying the transient nucleation theory just described, are able to quantitatively match the freezing kinetics observed in all of the dynamic compression experiments we present in both the main text and in the SM by the assignment of $\zeta = 55$. The instantaneous value of $\partial\phi/\partial t$ is given by the KJMA equation [27–31] mentioned earlier:

$$\frac{\partial \phi}{\partial t} = 4\pi(1-\phi)\gamma(t)\int_0^t J(t')\left[\int_{t'}^t \gamma(t'')\mathrm{d}t''\right]^2 \mathrm{d}t'. \tag{6}$$

We solve Equation (6) together with the governing conservation equations by running the multiphysics hydrodynamics code Ares [37] coupled with our phase transition kinetics code Samsa. These codes and the various material models employed by them are detailed in the SM.

Before the ramp compression path in the experimental study of Dolan et al. [10] has crossed the melt curve, the liquid is stable since $\Delta\mu = \mu_{\mathrm{solid}} - \mu_{\mathrm{liquid}} > 0$ [Figure 3(a)]. This is followed by a period of about 50 ns during which the water remains as a metastable liquid so that $\Delta\mu/k_{\mathrm{B}}T$, τ, and the critical cluster size n^* continue to decrease. Finally, when the magnitude of the driving force reaches a sufficiently large value of $|\Delta\mu/k_{\mathrm{B}}T| \approx 1$, freezing rapidly goes to completion (ϕ rises from 0 to 1) in about 10 ns, which is reflected in the sharp rise and fall of J. Optical transmission and imaging data from Dolan et al. also indicate that freezing is completed within about 10 ns. During the transition, the pressure decreases (from about 7 GPa to 6.7 GPa), which is consistent with freezing to the more dense ice VII phase. It is apparent from Figure 3 that both transient nucleation and the dual-temperature model are necessary to properly describe freezing at these extreme conditions. Our value of $\zeta = 55$ in Equation (5) results in a τ such that $I(t)$ suppresses the nucleation rate J to yield good agreement with Dolan et al. The figure also shows that if we neglect the fact that the growth rate is faster than the rate of latent heat transport so that both phases are described by a single temperature in which the liquid is hotter than it would be in reality (and hence, nucleation would be suppressed), then the resulting pressure profile does not match Dolan et al. and freezing does not achieve completion.

Our CNT-based solidification kinetics framework also quantitatively reproduces the results of a different class of experiments that utilize multiple-shock compression (Figure 4). The wave profile retains an idealized ringing structure in the absence of a transition, but if freezing does occur, there is again a rapid drop in pressure. Like in ramp compression, freezing achieves completion in multiple-shock compression, but it does so over 20-30 ns rather than $\approx$ 10 ns like in ramp compression. This is because the quasi-isentrope in multiple-shock compression attains higher temperatures (lower driving force) and so is less favorable for freezing. It is worth noting that in the multiple-shock data illustrated in Figure 4, there is a significant damping on the ringing immediately following the onset of freezing. This unknown source of dissipation is not accounted for by the phase transition kinetics alone and, although not the focus of our study, we have attempted to model the damping through a strength model for ice VII that we describe further in the SM.

Figure 4 also depicts results for an experiment with sapphire windows where the peak pressure is only around 5 GPa. Our models correctly predict that freezing does not occur under these conditions. In contrast, previously published simulations of these "null result" experiments have artificially disallowed freezing by removing the ice VII phase from their EOS (i.e., running liquid-only models), rather than allowing a model of the kinetics to determine the final state [9, 11–13, 18]. The ability to reproduce this null result is an important test of our CNT-based framework, and we show in the SM that it successfully reproduces similar experiments from Dolan and Gupta et al. [9] and Stafford et al. [13]

We have explained how a theoretical framework built on CNT and growth, when combined with hydrodynamics simulations, provides quantitative agreement with experimental pressure wave profiles associated with nanosecond freezing kinetics of liquid water to ice VII via homogeneous nucleation. This is the first such demonstration of a single, unified framework that can match the phase transition kinetics observed in multiple different dynamic compression experiments. Our results suggest new experiments regarding the nature of the metastability limit: if one were to increase the ramp-compression loading rate, could liquid water remain beyond 7 GPa? In opposition to this limit is the fact that faster loading rates also generate more entropy and thus reduce the driving force; therefore, there may be an optimal loading rate which can truly achieve the metastability limit. Such future studies, in-

formed by the results presented here, will shed light on the details of nucleation far-from-equilibrium and experimentally determine the limit where classical theory breaks down.

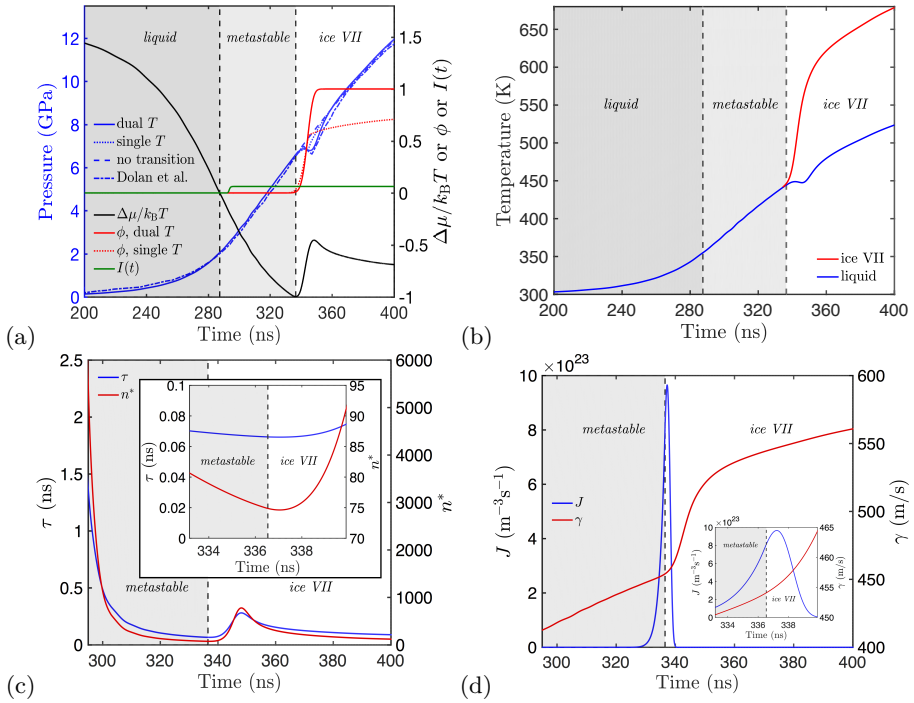

FIG. 3. Our simulation results for the ramp compression experiment of Dolan et al. [10] All of the results correspond to those from our dual-temperature model unless otherwise indicated. Panel (a) compares the pressure wave profile for 4 cases: three of which are from our simulations run with different models and the fourth is from Dolan et al. To aid in understanding, (a) also shows how the driving force $\Delta\mu/k_BT$, the ice VII phase fraction ϕ, and the transient nucleation factor $I(t)$ evolve with time. Panel (b) portrays the temperature in the two phases, (c) illustrates the induction time τ and number of ice molecules n^* in critical size clusters, and (d) depicts the nucleation rate J and growth rate γ, including insets that focus on the behavior near the onset of the transition.

Acknowledgments This work was performed under the auspices of the U.S. Department of Energy by Lawrence Livermore National Laboratory under Contract DE-AC52-07NA27344. We thank A. Arsenlis, D.P. McNabb, and B. Wallin for program and funding support, B.S. Pudliner for computational support regarding Ares, P.A. Sterne for EOS support on aluminum, and A.S. Connell and J. Long for their assistance with rendering Figure 1.

* belof1@llnl.gov

[1] J. Lindl, Phys. Plasmas **2**, 3933 (1995).
[2] Y. Bi, B. Cao, and T. Li, Nature Commun. **8**, 15372 (2017).
[3] A. Haji-Akbari and P. G. Debenedetti, J. Chem. Phys. **147**, 060901 (2017).
[4] L. Lupi, A. Hudait, B. Peters, M. Grünwald, R. G. Mullen, A. H. Nguyen, and V. Molinero, Nature **551**, 218 (2017).
[5] J. A. Sellberg, C. Huang, T. A. McQueen, N. D. Loh, H. Laksmono, D. Schlesinger, R. G. Sierra, D. Nordlund, C. Y. Hampton, D. Starodub, D. P. DePonte, M. Beye, C. Chen, A. V. Martin, A. Barty, K. T. Wikfeldt, T. M. Weiss, C. Caronna, J. Feldkamp, L. B. Skinner, M. M. Seibert, M. Messerschmidt, G. J. Williams, S. Boutet, L. G. M. Pettersson, M. J. Bogan, and A. Nilsson, Nature **510**, 381 (2014).
[6] C. Marcolli, Sci. Rep. **7**, 16634 (2017).

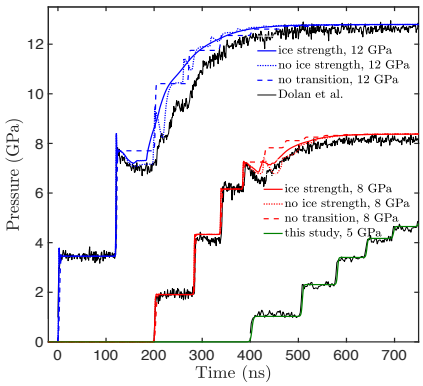

FIG. 4. Comparison between our simulation results and three multiple-shock experiments from Dolan et al. [10] The peak pressure is high enough for the transition to occur in the 8 and 12 GPa experiments, but not in the 5 GPa one. With the exception of the no transition curves (dashed), all of our results are produced with the dual-temperature model. The simulations include a plasticity model for the strength of ice VII that is active after solidification (solid blue and red curves) and results in a damping of the shock wave ringing after 400 ns (8 GPa) and 180 ns (12 GPa), in closer agreement with the experimental data than without strength (dotted curves).

[7] D. H. Dolan and Y. M. Gupta, Chem. Phys. Lett. **374**, 608 (2003).
[8] D. H. Dolan and Y. M. Gupta, J. Chem. Phys. **121**, 9050 (2004).
[9] D. H. Dolan, J. N. Johnson, and Y. M. Gupta, J. Chem. Phys. **123**, 064702 (2005).
[10] D. H. Dolan, M. D. Knudson, C. A. Hall, and C. Deeney, Nature Phys. **3**, 339 (2007).
[11] M. Bastea, S. Bastea, J. E. Reaugh, and D. B. Reisman, Phys. Rev. B **75**, 172104 (2007).
[12] S. J. P. Stafford, *An Experimental Study on the Dynamic Compression and Subsequent Freezing of Water*, Ph.D. thesis, Imperial College London, Department of Physics (2016), 223 pp.
[13] S. J. P. Stafford, D. J. Chapman, S. N. Bland, and D. E. Eakins, AIP Conference Proceedings **1793**, 13005 (2017).
[14] A. E. Gleason, C. A. Bolme, E. Galtier, H. J. Lee, E. Granados, D. H. Dolan, C. T. Seagle, T. Ao, S. Ali, A. Lazicki, D. Swift, P. Celliers, and W. L. Mao, Phys. Rev. Lett. **119**, 025701 (2017).
[15] P. C. Myint, L. X. Benedict, and J. L. Belof, J. Chem. Phys. **147**, 084505 (2017).
[16] R. B. Wordsworth, F. Forget, F. Selsis, E. Millour, B. Charnay, and J.-B. Madeleine, Astrophys. J. **733**, L48 (2011).
[17] A. R. Howe and A. S. Burrows, Astrophys. J. **756**, 176 (2012).
[18] P. C. Myint and J. L. Belof, J. Phys. Condens. Matter **30**, 233002 (2018).
[19] P. W. Bridgman, J. Chem. Phys. **5**, 964 (1937).
[20] O. Tschauner, S. Huang, E. Greenberg, V. B. Prakapenka, C. Ma, G. R. Rossman, A. H. Shen, D. Zhang, M. Newville, A. Lanzirotti, and K. Tait, Science **359**, 1136 (2018).
[21] D. Kashchiev, *Nucleation: Basic Theory with Applications*, 1st ed. (Butterworth-Heinemann, Oxford, 2000).
[22] A. A. Chernov, E. I. Givargizov, K. S. Bagdasarov, V. A. Kuznetsov, L. N. Demianets, and A. N. Lobachev, *Modern Crystallography III: Crystal Growth*, edited by H.-J. Queisser, Springer Series in Solid-State Sciences, Vol. 36 (Springer-Verlag, Berlin and Heidelberg, 1984).
[23] S. Toschev, "Homogeneous nucleation," (North-Holland Publishing, Amsterdam, 1973) Chap. 1 of Crystal Growth: An Introduction, pp. 1 – 49.
[24] E. Clouet, "Modeling of nucleation processes," (ASM Handbook, 2009) pp. 203–219.
[25] K. F. Kelton and A. L. Greer, *Nucleation in Condensed Matter: Applications in Materials and Biology* (Pergamon Publications, Oxford, 2010).
[26] C. N. Nanev, "Theory of nucleation," (Elsevier, Amsterdam, 2014) Chap. 7 of Handbook of Crystal Growth. Fundamentals: Thermodynamics and Kinetics., pp. 316–358.
[27] A. N. Kolmogorov, Izv. Akad. Nauk. SSSR Ser. Mat. **3**, 355 (1937).
[28] A. N. Kolmogorov, "On the statistical theory of metal crystallization," (Springer, Dordrecht, 1992) Chap. 22 of Selected Works of A. N. Kolmogorov. Volume II: Probability Theory and Mathematical Statistics, pp. 188–192, Shiryayev, A. N. (Ed.), Lindquist, G. (Trans.).
[29] W. A. Johnson and R. F. Mehl, Trans. Metall. Soc. AIME **135**, 416 (1939).
[30] M. Avrami, J. Chem. Phys. **7**, 1103 (1939).
[31] M. Avrami, J. Chem. Phys. **8**, 212 (1940).
[32] J. Q. Broughton, G. H. Gilmer, and K. A. Jackson, Phys. Rev. Lett. **49**, 1496 (1982).
[33] L. V. Mikheev and A. A. Chernov, J. Crystal Growth **112**, 591 (1991).
[34] L.-C. Valdès, J. Gerges, T. Mizuguchi, and F. Affouard, J. Chem. Phys. **148**, 014501 (2018).
[35] K. F. Kelton, A. L. Greer, and C. V. Thompson, J. Chem. Phys. **79**, 6261 (1983).
[36] D. Kashchiev, Surf. Sci. **14**, 209 (1969).
[37] B. S. Ryujin, in *DOE High Performance Computing Operational Review (HPCOR) on Scientific Software Architecture for Portability and Performance*, LLNL-CONF-676576, Gaithersburg, MD, USA (U.S. Department of Energy, 2015).
[38] See the Supplemental Material [`https://journals.aps.org/prl/`] for additional details on the nucleation rate and growth models, constitutive material models (equations of state, interfacial tension, diffusivity, strength), and the numerical simulations (time step and grid convergence results). The Supplemental Material

includes References 39–69 below.
[39] Z. Jian, N. Li, M. Zhu, J. Chen, F. Chang, and W. Jie, Acta Mater. **60**, 3590 (2012).
[40] D. P. Woodruff, "The structure of the solid-liquid interface," (Cambridge University Press, London, 1973) Chap. 3 of The Solid-Liquid Interface, pp. 39–62.
[41] F. Spaepen, Acta Metall. **23**, 729 (1975).
[42] F. Spaepen and R. B. Meyer, Scripta Metall. **10**, 257 (1976).
[43] G. W. Lee, W. J. Evans, and C.-S. Yoo, Phys. Rev. B **74**, 134112 (2006).
[44] E. H. Abramson, J. M. Brown, and L. J. Slutsky, J. Chem. Phys. **115**, 10461 (2001).
[45] A. A. Correa, L. X. Benedict, D. A. Young, E. Schwegler, and S. A. Bonev, Phys. Rev. B **78**, 024101 (2008).
[46] L. Burakovsky and D. L. Preston, J. Phys. Chem. Solids **65**, 1581 (2004).
[47] J. R. Gladden, J. H. So, J. D. Maynard, P. W. Saxe, and Y. Le Page, Appl. Phys. Lett. **85**, 392 (2004).
[48] L. M. Barker and R. E. Hollenbach, J. Appl. Phys. **41**, 4208 (1970).
[49] B. J. Jensen, G. T. Gray III, and R. S. Hixson, J. Appl. Phys. **105**, 103502 (2009).
[50] G. I. Kanel, W. J. Nellis, A. S. Savinykh, S. V. Razorenov, and A. M. Rajendran, J. Appl. Phys. **106**, 043524 (2009).
[51] D. G. Archer, J. Phys. Chem. Ref. Data **22**, 1441 (1993).
[52] W. M. Yim and R. J. Paff, J. Appl. Phys. **45**, 1456 (1974).
[53] G. H. Watson Jr. and W. B. Daniels, J. Appl. Phys. **52**, 956 (1981).
[54] R. M. More, K. H. Warren, D. A. Young, and G. B. Zimmerman, Phys. Fluids **31**, 3059 (1988).
[55] D. A. Young and E. M. Corey, J. Appl. Phys. **78**, 3748 (1995).
[56] D. A. Young, *Phase Diagrams of the Elements* (University of California Press, Berkeley and Los Angeles, 1991).
[57] C. A. Hall, J. R. Asay, M. D. Knudson, W. A. Stygar, R. B. Spielman, T. D. Pointon, D. B. Reisman, A. Toor, and R. C. Cauble, Rev. Sci. Instrum. **72**, 3587 (2001).
[58] D. Turnbull, J. Appl. Phys. **21**, 1022 (1950).
[59] B. B. Laird, J. Chem. Phys. **115**, 2887 (2001).
[60] A. Samanta and J. L. Belof, J. Chem. Phys. **Accepted** (2018).
[61] J. L. F. Abascal, E. Sanz, R. García Fernández, and C. Vega, J. Chem. Phys. **122**, 234511 (2005).
[62] D. Chandler, J. Chem. Phys. **62**, 1358 (1975).
[63] D. L. Preston, D. L. Tonks, and D. C. Wallace, J. Appl. Phys. **93**, 211 (2003).
[64] J. W. Swegle and D. E. Grady, J. Appl. Phys. **58**, 692 (1985).
[65] E. M. Schulson, Acta Metall. Mater. **38**, 1963 (1990).
[66] D. H. Dolan, "Private communication," May 11, 2016.
[67] T. V. Kolev and R. N. Rieben, J. Comput. Phys. **228**, 8336 (2009).
[68] E. J. Caramana, M. J. Shashkov, and P. P. Whalen, J. Comput. Phys. **144**, 70 (1998).
[69] P. C. Myint, B. Sadigh, L. X. Benedict, A. A. Chernov, B. M. Hall, and J. L. Belof, In preparation (2018).